HD^+ in a beam in intense pulsed laser fields: Dissociation and ionization with high-energy resolution of the fragments

Andreas Kiess, Domagoj Pavičić, Theodor W. Hänsch, and Hartmut Figger*
Max-Planck-Institut für Quantenoptik, Hans-Kopfermannstrasse 1, 85748 Garching, Germany
(Received 2 October 2006; revised manuscript received 20 December 2007; published 8 May 2008)

The isotopically mixed hydrogen molecular ion HD^+ was investigated in intense pulsed laser fields with high, i.e., vibrational resolution of the fragments. An ion beam of HD^+ with a translational energy of 11.1 keV was exposed to femtosecond laser pulses (100 fs) of intensities in the range from 10^{13}–10^{15} W/cm^2. Fragments from the two dissociation channels $HD^+ \rightarrow H+D^+$, and $HD^+ \rightarrow D+H^+$, as well as the Coulomb explosion channel, $HD^+ \rightarrow H^+ + D^+ + e^-$, were projected onto a two-dimensional multichannel plate detector to measure their velocity distributions. The fragments from the three channels were spatially clearly distinguished because of the different velocities of H (H^+) and D (D^+) fragments. Fragments from most of the populated vibrational states of HD^+ can be discerned as well-resolved peaks in the speed and angular distributions. The typical light induced potential (LIP) effects such as bond softening and level shifting already observed in the studies of H_2^+ and D_2^+ are here also observed. In addition to these one-photon peaks, also peaks due to three- (net two-) and finally also to direct two-photon absorption, typical of the asymmetric HD^+, were found in the vibrationally resolved fragment spectra of the dissociation channels. Besides the fragments from one-photon bond softening, also fragments formed by two- and three-photon processes were found to have narrow angular distributions, in contrast to the approximately $\cos^2$ distribution of fragments from vibrational levels above the LIP crossing being fragmented by classical dissociation. The relative probability of the two dissociation channels was investigated, addressing the question of the higher electron affinity to the proton or the deuteron during the dissociation, but could not be decided because of too low accuracy here. The Coulomb explosion channel was also clearly discerned by its fragment velocities as well as the narrow angular distributions of H^+ and D^+ fragments, which is quite analogous to those found in the cases of H_2^+ and D_2^+.

DOI: 10.1103/PhysRevA.77.053401 PACS number(s): 33.80.Rv, 33.80.Gj, 42.50.Hz

I. INTRODUCTION

During the last two decades elementary molecules such as H_2^+, D_2^+, Na_2, I_2, etc., were investigated in intense ultrashort laser pulses both theoretically and experimentally by measuring the kinetic energies of their nuclear and electronic fragments [1–3]. The isotopically mixed HD^+ is possibly the most interesting isotopic variant of hydrogen molecular ions. Since it is composed of a proton and a deuteron bound by one electron, the symmetry under the exchange of nuclei is lost. Unlike homogenous H_2^+ and D_2^+, it possesses a permanent electric dipole moment and is therefore infrared active, i.e., it absorbs and emits resonant IR radiation due to transitions between rovibrational levels of the ground electronic state. This electric dipole moment of the ground state $1s\sigma^2\Sigma$ of HD^+ was calculated in 1974 by Saha [4] and Bunker [5] to be 0.86 Debye and 0.87 Debye, respectively. In 1999 electric dipole moments for excited states of HD^+ were calculated by Moss [6]. The transition dipole moments were estimated to be an order of magnitude smaller by these authors. In storage rings, such as the one at the MPI für Kernphysik in Heidelberg, Germany, these ions were circulating for 350 ms until they had deactivated to their vibrational ground state by IR radiation [7,8]. Then they were merged for neutralization with velocity matched electrons to study their following dissociative recombination.

The subject of the present contribution is to investigate HD^+ by an ion beam fragmentation method in intense femtosecond laser fields with intensities between 10^{13} W/cm^2 and 10^{15} W/cm^2. The first and also the most experiments of that kind were performed on H_2^+ and D_2^+ starting with neutral H_2 and D_2 with laser pulses around 100 fs and intensities of up to 10^{15} W/cm^2 [1,2]. Here formation of H_2^+ and its fragmentation were done in one laser pulse, i.e., the first electron is ionized at the rising edge of the laser pulse and the resulting H_2^+ is then fragmentized around the peak of this pulse. Later on, however, it turned out that the assumption made that the two processes are independent is not justified when investigating finer details of the fragmentation.

Both dissociation, such as $H_2^+ \rightarrow H+H^+$, and Coulomb explosion, $H_2^+ \rightarrow H^+ + H^+ + e^-$, were found as decay channels in the intense fields. The translational energies of the fragments were in most experiments measured by the time-of-flight (TOF) method. The spectra measured were found to be almost unstructured in contrast to theoretical investigations, e.g., [9]. Usually no angular fragment distributions were reported.

It was an important step forward when supersonic molecular beams of H_2 and D_2 [10], and in particular ionic beams of Ar_2^+ and the hydrogen isotopomers H_2^+ and D_2^+ were exposed to strong laser fields [11–14]. In the latter experiments the ions were generated in a dc-discharge source and accelerated to keV energies. After mass separation and high collimation, the beams were exposed to the focused laser beams. The resulting fragments were investigated by the TOF method [14] or by imaging of their velocity distribution

*Author to whom correspondence should be addressed: figgerhartmut@web.de

on a position-sensitive detector [11–13]. In addition to the main progress of performing the experiment directly on the mass selected molecular ions with known vibrational population distribution, also a higher kinetic energy resolution could be reached by the later technique [13,15]. As a consequence, structure in the fragment velocity distribution reflecting vibration of the parent molecules was discovered in the dissociation channel. This enabled the authors to investigate with vibrational resolution the special effects of the light induced potential (LIP) theory—bond softening, level shifting, and trapping of the H_2^+ and D_2^+ ions in the new potentials. Ben-Itzhak *et al.* recently improved the ion-beam technique by developing a three-dimensional (3D) momentum imaging technique that measured the H_2^+ fragments in coincidence [16]. Only recently, a clear structure was also found in the Coulomb explosion channel which allowed the charge-resonance enhanced ionization (CREI) model [17] to be tested in unprecedented detail [18,19].

When extending the ion beam method to HD^+ [20,21], deviating from H_2^+ and D_2^+, we observe that this isotopomer has three fragmentation channels, namely two dissociation channels

$$HD^+ \rightarrow H^+ + D(1s), \tag{1a}$$

$$HD^+ \rightarrow H(1s) + D^+, \tag{1b}$$

and the Coulomb explosion channel

$$HD^+ \rightarrow H^+ + D^+ + e^-. \tag{2}$$

The isotopic difference in HD^+ as compared to H_2^+ has the effect that the threshold for channel (1a) is 3.7 meV lower in energy than that of channel (1b) in the dissociation (large R) limit (Fig. 1). This was found to be attributed to the finite nuclear mass correction to the Born-Oppenheimer (BO) approximation. This "breakdown" of the Born-Oppenheimer approximation has been studied, for example, by Carrington *et al.* [22] using microwave spectroscopy of HD^+ near the dissociation limit. Their measurements are in agreement with *ab initio* structure calculations only upon inclusion of corrections to the BO approximation. By hyperfine splitting measurements the authors also found that the electron prefers to be located near the deuteron for vibrational levels of HD^+ close to the dissociation limit.

Ben-Itzhak *et al.* [23] and Wells *et al.* [24] determined the branching ratio of the dissociation channels (1a) and (1b) to be asymmetric by 7% in favor of the energetically lower channel (1a). To that aim they ionized the HD molecule by fast proton impact to produce a vibrational continuum of the HD^+ ground electronic state, followed by dissociation into channels (1a) and (1b). The authors find their experimental results to be consistent with their coupled channels calculation and with a model based on Meyerhof's approximate formulation [24].

Our ion beam method mentioned above, in principle offers a way to do similar studies in the dissociation channels' asymmetry. In this work we have observed all three channels (1a), (1b), and (2). Their branching ratios in principle can be compared since they appear, to a large degree, to be spatially separated on the detector. Since our method strongly deviates from that of Wells *et al.* [24], our results also may differ a lot. Unfortunately the accuracy we reached here so far is insufficient (Sec. IV G).

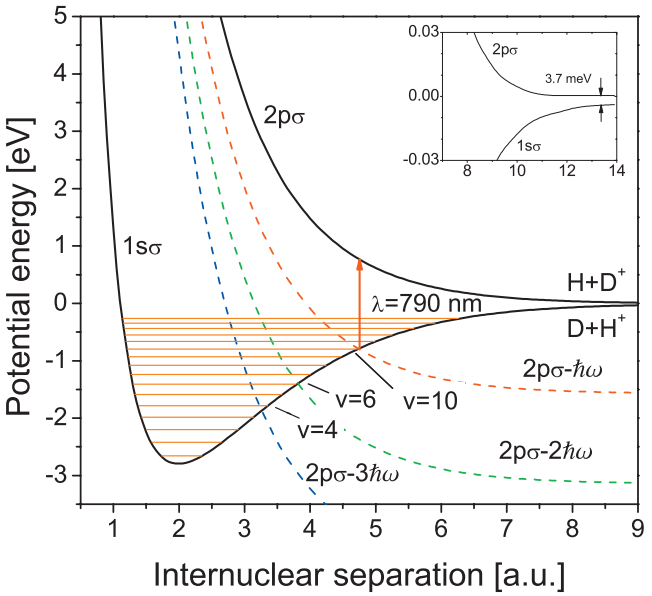

FIG. 1. (Color) The unperturbed potential curves $1s\sigma$ and $2p\sigma$ of HD^+. The dashed lines indicate the $2p\sigma$ curve shifted by one-, two-, and three-photon energies, leading to three crossings with the $1s\sigma$ curve in the vicinity of the vibrational levels $v=4$, $v=6$, and $v=10$. In the strong-field regime, gaps open up at these crossings (so-called anticrossings) and molecules from the vibrational levels below the crossings start to dissociate by so-called bond softening.

Charron *et al.* theoretically studied the photodissociation of HD^+ in an intense linearly polarized laser pulse using a time-dependent wave-packet approach [25]. Application of a coherent superposition of the fundamental radiation and its second harmonic leads to asymmetries in the angular distributions of H^+ and D^+. Sheehy *et al.* performed corresponding experiments to coherently control photodissociation by phase dependence of the spatial asymmetry of the fragment spectrum [26]. The authors claim that they thereby established new methods of control of chemical reactivity and isotope separation.

Recently Roudnev *et al.* calculated effects of the carrier-envelope phase (CEP) difference of an ultrashort (10 fs) laser pulse on dissociation of HD^+. Starting from the time-dependent Schrödinger equation they demonstrated that the branching ratio of channels (1a) and (1b) depends on the phase, and that either of the two channels can be made dominant by the CEP variation by more than a factor of 2 [27]. The same group later on improved this calculation on HD^+ using a "scaled coordinate approach" in three dimensions [28]. They also derived the fragments' translational energy spectra for the case of HD^+ from the density function for a 10 fs laser pulse at 790 nm.

The permanent dipole moment of HD^+ also can play a special role in the trapping of this molecule by an IR laser field, which is known as dynamical dissociation quenching. In this mechanism, the trapping is based on the synchronization of the inner molecular motions and the laser field oscillations [25,29]. This effect should not be mixed up with the

Floquet trapping, which was first theoretically investigated in the case of H_2^+.

Numerous further spectroscopic experiments and calculations were performed on this fundamental molecular system which is impressively reviewed by Carrington *et al.* [30]. The knowledge of the rovibronic levels is of special interest for the present work and was taken from Wolniewicz and Poll [31]. The vibrational populations of HD^+, H_2^+, and D_2^+ formed by electron impact on HD, H_2, and D_2, respectively, are reported in [32,33] and are expected to be close to ours.

The infrared absorption spectrum due to transitions between rovibrational levels of the electronic ground state of HD^+, $1s\sigma^2\Sigma$, in the wavelength range from 5.1 to 6 μm, was detected by Wing *et al.* [34]. Using an ion beam laser resonance method, a resolution of 10^{-6} was reached allowing to partly resolve the hyperfine structure of the rovibronic levels.

Finally we want to mention a recent study on H_2^+ and HD^+ concerning a precision investigation of fundamental constants, performed by Roth *et al.* [35] who measured at millikelvin temperatures rovibrational transitions with a resolution of $\leq 10^{-9}$. To that aim those molecules were stored in a radio-frequency trap and sympathetically cooled down to ~ 20 mK using laser cooled Be^+ ions. The authors are investigating QED effects of this fundamental three-body quantum mechanical system by comparison to *ab initio* calculation, as well as the fundamental constant m_e/m_p and its variation with time. Frequency combs in the IR developed very recently will be used for these precision measurements.

II. THEORY

As already mentioned in the Introduction, the heteronuclear molecular ion HD^+, as an isotopomer of the smallest molecules in nature H_2^+ and D_2^+, consists of a proton and a deuteron bound by one electron. The inner molecular forces are approximately described by a potential curve system consisting of a bonding ground electronic state of the $1s\sigma$ type and a dissociative $2p\sigma$ state (Fig. 1). This is a rather pure two-state system since the next higher electronic states are about 11 eV higher in energy. Deviating from the homonuclear H_2^+ (D_2^+) case, the two potential curves are not asymptotically degenerate at large nuclear distances R, but the degeneracy is lifted by 29.8 cm^{-1} (3.7 meV). This is a consequence of the coupling of the electronic and the nuclear moments due to the small dipole moment caused only by the nuclear mass difference. Dissociation of the ground state leads to the products $H(1s)+D^+$ [channel (1b)], whereas on the dissociative curve $2p\sigma$ the products are $H^+ + D(1s)$ [channel (1a)]. This means that in the first case the electron decides to join the proton and in the second case the deuteron. As already mentioned in the Introduction, manipulation and investigation of the dissociative branching ratios in this simplest molecule (e.g., by the phase control between a laser field and its first harmonic) is of great interest and is an example of the breakdown of the Born-Oppenheimer approximation [25,26].

Numerical solutions of the Schrödinger equation for HD^+, including the complete Hamiltonian with all the electric dipole interactions are reported in Refs. [36,37]. In the following, results of a theoretical treatment are more phenomenologically introduced and used for qualitative and partly quantitative explanations of the effects observed in the velocity distributions of the HD^+ fragments.

While the two-potential curve system shown in Fig. 1 as discussed above principally remains valid for perturbations by small electromagnetic fields, the intense-field experiment reported in the present contribution must be interpreted by the "dressed" states or Floquet model (see e.g., [1,2]). Here the laser light field is no longer treated as a perturbation in the relevant Hamiltonian, but the light field and its interaction with the molecule, and in particular its electric dipole moment, must be fully included in the diagonalization of the Hamiltonian. If this procedure is started only with the two lowest electronic states (i.e., $1s\sigma$ and $2p\sigma$), it results in so-called diabatic potential curves, $W_{1,2}(R)$. They are derived from the unperturbed curves $E_{1,2}(R)$ by shifting them by multiples n of the photon energy, $W_{1,2}=E_{1,2}+nh\nu$. However, the new light-induced (so-called adiabatic) potential curves, $E_{\pm}$, for the case of one-photon absorption ($n=1$) are

$$E_{\pm}(R) = \frac{1}{2}\{E_1(R) + E_2(R) + \hbar\omega_L \pm \sqrt{[E_1(R) + \hbar\omega_L - E_2(R)]^2 + (\hbar\omega_R)^2}\}, \tag{3}$$

where ω_R is the Rabi frequency, $\omega_R = \langle\phi_i|\boldsymbol{D}\cdot\boldsymbol{E}|\phi_j\rangle/\hbar$. Here ϕ_i and ϕ_j are the wave functions of the unperturbed molecular system, $\boldsymbol{D}$ is the transition dipole moment, $\boldsymbol{E}$ is the laser electric field and ω_L is the laser frequency. The curves $E_{\pm}(R)$ arise from the unperturbed curves $E_{1,2}(R)$ by adding one-photon energy to $E_{1,2}(R)$ and including the repulsion part, which changes the crossing to an avoided crossing. In Fig. 1 for simplicity only the relevant diabatic potential curve system is given, in which the vibrational level $v=10$ is closest to the one-photon crossing. Roughly speaking, the new curves, usually called light induced potentials, are generated by the bonding part of $E_1(R)$ and a dissociative part of $E_2(R)$. These two unperturbed states start to mix when $\hbar\omega_R \approx \hbar\omega_v$, where ω_v is the vibrational frequency. They are illustrated principally and intensively discussed in [1] (p. 93, Fig. 2.8 and p. 159, Fig. 3.5), however for different laser wavelengths. The laser-induced shapes of the potential curves $E_{\pm}(R)$ are the reason for the new effects occurring in intense fields, such as bond softening, vibrational level shifting, tunneling and vibrational trapping (bond hardening). The vibrational levels lying inside the laser formed gap(s) below the crossing(s) of the diabatic potential lines are not only strongly dissociated but are also energetically strongly shifted compared to their weak field, "classical" energetic positions, which is the so-called "level shifting" effect. The levels tunneling through the lower LIP part, $E_-(R)$ are also strongly shifted. However, the ones coinciding energetically exactly with the crossing(s) are unshifted according to the LIP theory. These effects were confirmed for the relevant vibrational levels in our former works on H_2^+ and D_2^+ [13,15].

The higher-order process, namely the net two-photon absorption has also been detected and vibrationally resolved in

our recent study of H_2^+ and D_2^+ [38,39]. In this process three photons are absorbed as indicated by the crossing of $E_1(R)$ with three-photon dressed potential curve $E_2(R)$ at about $v=4$. Since this curve at higher R crosses a $1s\sigma$ curve dressed with two photons, one photon is re-emitted and the fragments come out as having effectively absorbed two photons. This dissociation path is also present in H_2^+ and D_2^+ and is illustrated, e.g., in [1] (page 98, Fig. 2.12) or in [15]. This opening of the gap at about $v=4$ can be detected if the peak laser intensity is increased. The mathematical treatment here is analogous to the one of the avoided crossing of the one-photon dressed curves.

While direct two-photon absorption is forbidden in H_2^+ as well as in D_2^+ because of parity selection rules, it is allowed in HD^+ because of its intrinsic permanent transition dipole moment. This allows transitions between rovibrational levels within the ground electronic state, e.g., $E_1(R)$ and, in a next step, by absorption of a second photon, by another dipole transition, to the continuum. Consequently in the LIP picture there is a third crossing of $E_1(R)$ with a two-photon dressed curve at about $v=6$, see Fig. 1. The opening of the gap at this crossing at sufficiently high laser intensities should result in the fragments with $v=6$ and $v=5$.

LIP curves for HD^+ were calculated by Datta *et al.* for the laser wavelength of 329 nm [36]. Since the laser wavelength applied there differs much from ours (790 nm), their results are only qualitatively useful for this work. Despite that, the general formalism used there remains applicable.

Comparing the LIP systems of HD^+ to those of H_2^+ and D_2^+ [13], a qualitatively similar behavior of these ions must be expected concerning the intense-field effects mentioned above, irrespective of the fact that there are two different fragments now. However, appreciable differences due to the direct two-photon absorption effects because of the electric dipole transition moments between vibrational levels of the electronic ground state are expected.

III. EXPERIMENTAL SETUP

As already pointed out, we used an ion beam apparatus for the formation of a fast beam of the HD^+ ions (see Fig. 2 in Ref. [15]), which contrasts to most of similar intense-field dissociation experiments performed so far on hydrogen molecular ions. The ionic beam was generated by a dc electric discharge of commercially available HD gas in a hollow cathode duoplasmatron ion source. The gas pressure in the source was ~ 1 mbar. The discharge current and voltage were typically 100 mA and 400 V, respectively. The ions formed in the discharge were drawn out through a 200-μm-diameter opening in the anode and accelerated to typically 11.1 keV. The initially divergent beam was collimated by a lens system consisting of two electrostatic ion lenses (Einzel lenses) and mass selected by a sector magnetic field. Two pairs of perpendicular deflection plates placed before and after the sector field allowed the exact alignment of the beam through the beam defining apertures. The ion beam with a diameter of 1 mm was collimated down to a rectangular shape of 25×200 μm by two apertures separated by a distance of 53 cm.

In the electric discharge, besides HD^+ also the triatomics H_3^+ and D_3^+ are formed in appreciable densities. Since HD^+ and H_3^+ have the same mass, they cannot be separated in the mass selector described above and therefore both ions are present in the ion beam. Therefore the fragments observed in the experiment potentially originate from both parent molecular ions. To find out the contribution of H_3^+, an H_3^+ ion beam was formed in the ion source from pure H_2 gas and was exposed to intense laser pulses. Since at the intensities we used, no fragmentation of H_3^+ was found, its presence in the beam has no effect on the measured fragment distributions.

A linearly polarized pulsed femtosecond laser beam is focused onto the horizontally running ion beam. The axis of laser propagation, laser polarization, and the ion beam were all mutually orthogonal. The molecular ion is fragmentized by the laser pulse and the fragments are detected on a two-dimensional position-sensitive detector mounted perpendicularly to the ion beam axis. The detector assembly consists of two multichannel plates (MCPs) in a chevron configuration with an active diameter of 40 mm followed by a phosphor screen. The luminescent pattern on the phosphor screen resulting from the fragments impinging on the detector was imaged by a lens system on a 384×286 pixel charge coupled device (CCD) camera. In this way the projection of the fragment velocity distributions onto the detector plane is measured and stored by a computer. The pressure in the interaction chamber was about 10^{-8} mbar.

The femtosecond laser system was an all solid-state commercial setup (Spectra-Physics, Spitfire). It consists of a Ti:sapphire oscillator at a central wavelength of 790 nm and a repetition rate of 82 MHz. The oscillator seed pulses were amplified in a chirped pulse amplification (CPA) system, delivering 100-fs pulses with a repetition rate of 1 kHz and a maximum energy of 2 mJ. The laser intensity in the interaction zone was varied by shifting the focusing lens relative to the ion beam, thereby moving away the waist of the focused light from the perpendicularly crossing ion beam.

IV. RESULTS AND DISCUSSION

A. Generation of the data

Prior to the discussion of the measurements, details of their generation should be reported. First the CCD chip analogly stored the detected fragments generated by typically 7500 laser pulses by the pixels charge amount which was then digitized. Then during a time-delayed interval of the same duration the background was measured in the same way and subtracted. Such an image was stored in the PC. A complete measurement consists of the sum of 600 such images corresponding to 4.5×10^6 laser pulses. Since such a measurement of the fragment velocity distribution is fully symmetric to the axis perpendicular to the axis of laser polarization, one-half of the picture contains the full experimental information and therefore was only measured. The intention here was to use all the pixels of the CCD chip of the detector to reach the best velocity resolution. To obtain a complete result as shown in Fig. 2 the measurement so far

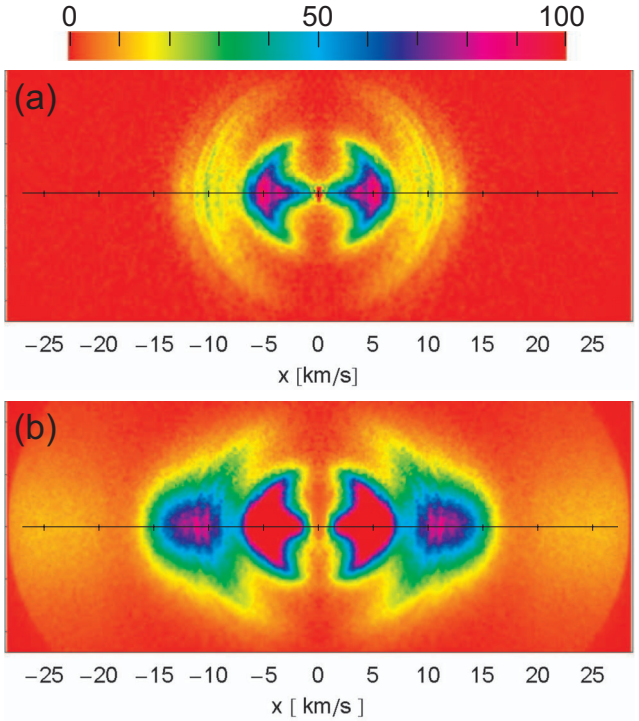

FIG. 2. (Color) The measured two-dimensional velocity distribution of (a) neutral fragments and (b) neutral together with charged fragments. The laser polarization is horizontal in the plane of the image. The laser intensity was 1×10^{15} W/cm^2 and the pulse length was 100 fs in both measurements. The scale in (a) indicated the fragment velocity in km/s along the horizontal axis. Only one-half of the distribution is measured, which was then mirrored along the axis perpendicular to the polarization axis. In (b) the Coulomb explosion fragments, D^+ (at velocities of 8–16 km/s) and H^+ (above 20 km/s) are clearly seen. In (b) the color scale was adjusted to show the H^+ Coulomb explosion channel.

described was computationally mirrored about the axis mentioned above.

For normalization of the measurements to the same number of parent HD^+ molecules, the ion beam current was recorded during the measurement using a tiny Faraday cup placed in front of the MCP. Unfortunately the cup screens a small portion around the center of the detector as can be noticed in Fig. 2.

B. Projection of the fragments

Upon interaction with the laser field, the fragments formed in channels (1a), (1b), and (2) gain the kinetic energy E from it. In case of dissociation, the energy E gained by the fragments is determined by the difference between the energy of the n photons absorbed, $nh\nu$, and the binding energy, E_v, of the particular rovibrational state v,

$$E = nh\nu + E_v, \quad E_v < 0. \tag{4}$$

The fragments with the same energy E [i.e., the fragments from the same rovibrational state in channels (1a) and (1b)] are distributed on the surface of an imagined sphere that expands while traveling toward the detector. The distribution of the fragments on the sphere is cylindrically symmetric with respect to the polarization axis. Initially the molecules in the beam are isotropically distributed. Their fragmentation proceeds along the nuclear axis. If dissociation probability is linear with laser intensity, which is the case in weak-field dissociation of the vibrational levels $v \geq 10$, the molecules under an angle θ with respect to the polarization axis experience the effective intensity $I_{\text{eff}}=I_0 \cos^2\theta$. Consequently, the distribution of the fragments on the sphere is $\cos^2$-like.

When this spherical fragment distribution is projected on the plane of the detector, a circularly shaped distribution interrupted along the line perpendicular to the polarization axis is generated, as shown in Fig. 2. In order to reconstruct the original three-dimensional distribution from the planar distribution on the detector plane, the so-called inverse Abel transformation must be applied [40]. The computational procedure was performed on a PC using an algorithm of Vrakking [41].

C. Velocities and energies of the fragments

The momentum conservation (neglecting the electron and photon momenta) requires, e.g.,

$$\boldsymbol{p}_{HD^+} = \boldsymbol{p}_H + \boldsymbol{p}_D, \tag{5}$$

where subscripts H and D stand for neutral or charged fragments. Because of the relatively small mass difference between the proton and the neutron, in the center-of-mass system of HD^+ ($\boldsymbol{p}_{HD^+}=0$) we have

$$m_H \boldsymbol{w}_H = -m_D \boldsymbol{w}_D, \quad E_H = 2E_D, \tag{6}$$

where $\boldsymbol{w}$ is fragment velocity in the molecular-ion reference frame. Therefore, the energy gained by absorption of the photon(s) [Eq. (4)] is distributed in the ratio 2:1 between H (H^+) and D (D^+). The expected "theoretical" velocities of the fragments coming from the different vibrational levels of HD^+ (drawn in all the radial speed distributions in Figs. 4 and 6 as perpendicular lines) are given by

$$w_H = \sqrt{4(h\nu + E_v)/(3m_H)}, \tag{7}$$

$$w_D = \sqrt{2(h\nu + E_v)/(3m_D)}. \tag{8}$$

Because of $w_D = w_H/2$, the H (H^+) and D (D^+) fragments coming from a certain vibrational level v are clearly separated. The energy of the laser photon at 791 nm is ~1.6 eV. The binding energies E_v of the vibrational levels v of HD^+ were taken from [31]. The deflection $Y_{H,D}$ of the fragments H (D) on the detector is

$$Y_{H,D} = w_{H,D} T. \tag{9}$$

Here T is the flight time of the fragments between the place of fragmentation and the detector,

$$T = d\sqrt{m_{HD^+}/(2E_{HD^+})}, \tag{10}$$

where d is the distance between these two places. The translational kinetic energy of the HD^+ ions is $E_{HD^+}=Q_{HD^+}U = 11.1$ keV, where Q_{HD^+} is the electric charge of HD^+ and U is the acceleration voltage.

Neutral and charged fragments of approximately the same mass (such as H and H^+) cannot be spatially separated on the detector. However, by deflecting charged fragments to the side by an electric field, measurements of only the neutrals can be performed.

D. Overview of the two-dimensional HD^+ fragments distributions

Figure 2 shows typical results of measurements of the fragment distribution of HD^+ for a relatively high laser intensity of 1×10^{15} W/cm^2. In the measurement in Fig. 2(a) the charged fragments were deflected in a Faraday cup and only the neutral H and D fragments from dissociation channels (1a) and (1b) are detected. In Fig. 2(b) velocity distributions of both neutral and charged fragments are shown. In both figures the H (H^+) and D (D^+) fragments are partly spatially separated. Since $w_H=-2w_D$, the D (D^+) fragments are positioned more to the midst and the H (H^+) fragments to the outer part of the MCP detector. The signal of the H (H^+) fragments appears weaker, since these fragments are distributed over a much larger area of the detector. Also the detection efficiency for the heavier D (D^+) fragments is larger than that of H (H^+) fragments by 10%–15% since they are impinging on the detector with a 2 times higher translational kinetic energy [42].

The H fragments farther outside at velocities between 8 and 11 km/s form a clear ringlike structure familiar from the experiments on H_2^+ and D_2^+ [13,15]. The rings originate from one-photon dissociation of molecules in different vibrational levels that energetically lie in and above the one-photon crossing. In particular the broad angular distribution being close to a $\cos^2$ distribution indicates a classical-like dissociation according to Fermi's golden rule. A similar distribution is also found for the D fragments from the vibrational levels of HD^+ in and above the one-photon crossing. The angularly narrow fragment distribution close to the origin results from bond softening of the levels below the crossing. In conclusion, the vibration of HD^+ becomes apparent in both dissociation channels, the higher vibrational levels being more clearly represented by the H fragments and the lower ones by the D fragments.

The measured distributions are varied when also the charged fragments are included [Fig. 2(b) and Fig. 6]: in addition to the H^+ and D^+ fragments from the dissociation channels, which only add up to and increase the signal at the corresponding neutrals, the charged fragments coming from the Coulomb explosion channel (2) are also detected now. Their effect can be studied by comparing Figs. 2(a) and 2(b): The H^+ from the Coulomb explosion channel land far outside at velocities above 20 km/s, while the D^+ fragments from this channel appear between 10 and 15 km/s. Because of the high laser intensity used here, no structure could be recognized in the Coulomb explosion channel as we observed in the kinetic energy distributions of H_2^+ and D_2^+ [19,43].

E. Discussion of the radial speed distributions: Single vibrational levels

In Figs. 2–6, a strong variation of the fragment distributions with laser light intensity is observed. By investigating the speed and angular distributions of the photofragments, the LIP effects as discussed in Sec. II could be qualitatively and partly quantitatively studied for the single vibrational levels.

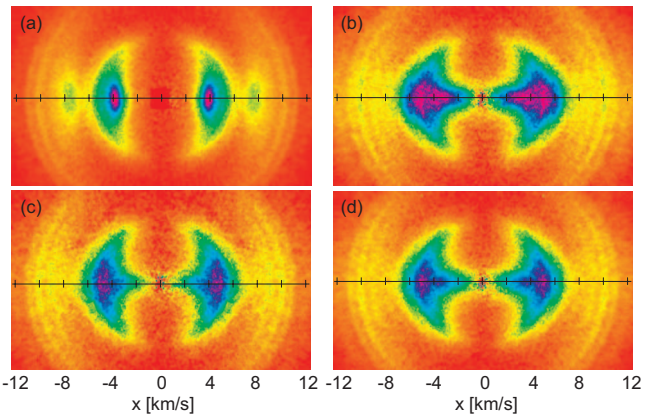

FIG. 3. (Color) Measured two-dimensional velocity distributions of the neutral photofragments. The peak laser intensities were 3×10^{13} W/cm^2 (a), 2×10^{14} W/cm^2 (b), 5×10^{14} W/cm^2 (c), and 1×10^{15} W/cm^2 (d). The maximum velocity along the horizontal axis is 12 km/s.

The two dissociation channels (1a) and (1b) are best investigated by the measurements in which only their representative neutral fragments H and D, respectively, are detected, and the Coulomb channel (2) represented by the charged fragments H^+ and D^+ is suppressed.

Figure 3 shows the two-dimensional (2D) distributions of neutral fragments for increasing laser intensities of 3×10^{13} -1×10^{15} W/cm^2. Figure 4 shows the corresponding radial speed distributions obtained by integrating the Abel-reconstructed 3D velocity distributions over $\pm4°$ around the polarization axis of the laser at each speed. These plots show a better speed resolution of the peaks than those in Figs. 5 and 6, where also the charged fragments are included in the corresponding plots of the two-dimensional and radial speed distributions, respectively. The reason for this might be that the neutral fragments are less disturbed on their way to the detector than the ions. In addition the H and H^+ (or D and D^+) contributing to the same peak come from the different dissociation channels (1a) and (1b) and therefore have different velocities, which also leads to a broadening of the peaks.

All the speed distributions in Fig. 4, as well as the ones in Fig. 6 show three, or in two measurements even four main broad maxima, which are interpreted in the following to be due to a special (or an additional admixing) LIP effect.

The broad maxima just mentioned show an additional substructure which in the following we can partly attribute to the vibrational levels. This will be done by comparison of the experimental velocity peak structure to the "classical" vibrational velocities of the fragments H (H^+) and D (D^+) represented as vertical lines ("combs") in the radial speed distributions, Figs. 4 and 6. These lines are calculated by using the kinetic energy E from Eq. (4) where $n=1,2$ gives the numbers of photons absorbed and E_v here is the classical, i.e., low-field binding energy of the vibrational levels v. On the basis of the LIP theory we interpret the coincidence with and

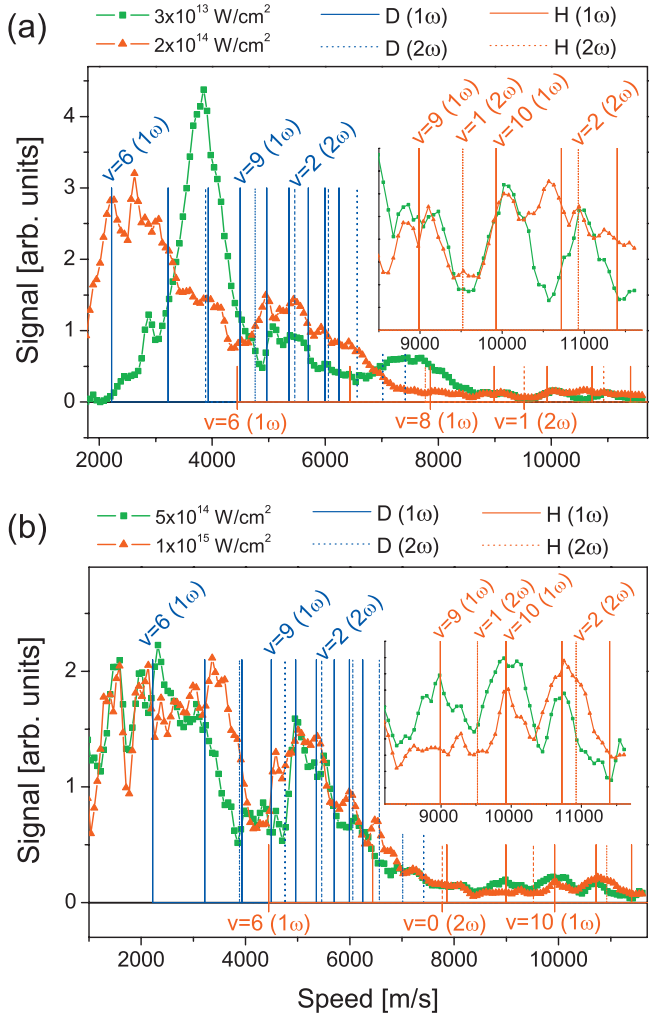

FIG. 4. (Color) Speed distributions of the neutral photofragments for the measurements in Fig. 3. The distributions were obtained by integrating the Abel-inverted velocity distributions over ±4° around the polarization axis at each speed. The vertical lines represent the classically expected velocities for the H and D fragments after one- and net two-photon absorption as calculated from Eq. (4).

in particular the deviations of the measured peak structure from these "classical" positions.

The Coulomb channel is experimentally suppressed in Figs. 3 and 4 as pointed out before. In Fig. 6 this channel is shown only by the D^+ fragments, since the velocities of the H^+ fragments are beyond the velocity range displayed. In all plots showing radial speed distributions, namely Figs. 4 and 6, combs displaying the velocities of the fragments H (H^+) and D (D^+) from the different vibrational levels for the weak-field (classical) case, are given by the vertical lines. Also such combs for two-photon absorption are included there. By these combs the peak structure in our spectra can be partly vibrationally assigned though, corresponding to the intense field theory, LIP, they are more or less shifted away from the classical positions. Here also the overlapping of H (H^+) and D (D^+) fragments, see (ii), as well as the broadening of the lines by the intense field must be respected. It should be noted that this is no deficit of our experimental method's resolution, but characteristic of intense field dissociation.

(i) The first big maximum at small speeds below 4000 m/s in Figs. 2–6, according to the comb, consists of D (Figs. 3 and 4) or $D+D^+$ (Fig. 6) fragments respectively, coming from the dissociation channels. It should be due to bond softening of the vibrational levels $v=6$ (or $v=7$) to $v=8$ (or $v=9$) caused by one-photon absorption (Figs. 4 and 6). This is supported by the narrow angular distribution of the fragments here as shown in Figs. 3 and 5 and will be also discussed in Sec. IV F. This maximum broadens and shifts with increasing intensity to lower velocities and therefore lower vibrational levels. This can be explained in the LIP picture by the increasing gap at $v=10$ (Fig. 1) between E_+ and E_- with growing intensity, in analogy to its isotopomers H_2^+ and D_2^+ [13,15].

Considering the lowest intensity measurement at 3×10^{13} W/cm^2 for the neutrals in Fig. 4 in more detail, the main feature at low velocities is the peak at about 3900 m/s which has a faint bump at its right-hand shoulder which is also observed in the plots of measurements with charged particles at similar intensities, e.g., in Fig. 6(a). When we tentatively attribute this very small feature to $v=9$ as proposed by the vibrational comb, the big peak at 3800 m/s should be ascribed to $v=8$. Alternatively, neglecting this faint feature at the right-hand shoulder, the large maximum might be caused by the shifted dissociating $v=9$ level. The two peaks on the left-hand shoulder observed here at again lower intensities might be due to the next lower shifted vibrational levels $v=7$ and $v=6$, or $v=8$ and $v=7$, respectively.

For higher intensities in Fig. 4(b) or Figs. 6(b) and 6(c) we do not try to assign vibrational levels to the structure of the first maximum below 4000 m/s because the result would be again more speculative: We can only state here that this maximum with increasing laser intensity is more and more formed by the dissociation of the lower vibrational levels $v=6-8$. Thereby it is moved to lower fragment velocities since a larger shift of the levels and a stronger broadening of the lines take place. The H (H^+) fragments from the levels $v=6-8$ due to bond softening are hidden in the second and third broad maximum as discussed below in (ii) and (iii) and cannot clearly be identified.

(ii) Now we consider the second broad maximum lying between 4500 and 7000 m/s in Figs. 4(a) and 4(b). According to the comb it is mainly formed by D fragments from channel (1a). This region mostly peaks at three or even four velocities: At about 5000, 5400, 5900, and 6200 m/s [see Fig. 4(a), peak intensity of 2×10^{13} W/cm^2]. These peaks shift a bit with changing intensity. From the comb the first two should be attributed to the levels $v=10$ and $v=11$ as observed best at lower laser intensities considering Fig. 4. These levels lie close to the crossing point at $v=10$ (gap) in the LIP curve system, Fig. 1, caused by one-photon absorption and can be rather uniquely assigned since they are not shifted with intensity. Furthermore, the D and D^+ fragments here show a broad angular distribution with an almost $\cos^2$ characteristic observed in Figs. 3 and 5 (left-hand column), the 3D display of the fragments confirming a classical dissociation as expected for these levels from the LIP curves.

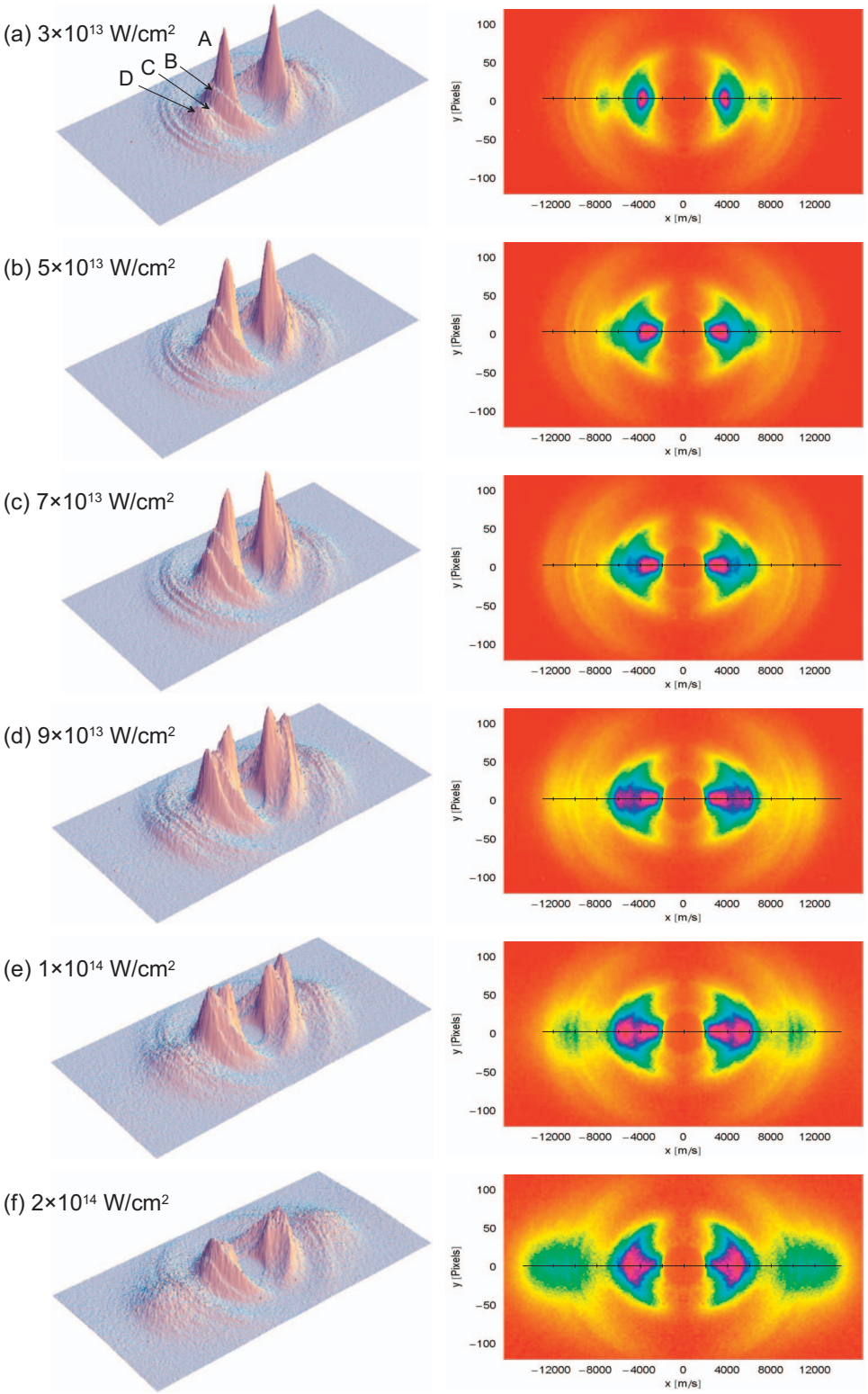

FIG. 5. (Color) Measured two-dimensional velocity distributions of the neutral and charged fragments together in three- (left-hand column) and two- (right-hand column) dimensional representation for laser intensities from 3×10^{13} W/cm^2 to 2×10^{14} W/cm^2. Each measurement contains fragments from about 4.5×10^6 laser pulses. The three-dimensional distributions on the left-hand side show most impressively the relative development of the four peaks being due to one-photon bond softening (*A*), "classical" one-photon (*B*), three- (net two-) photon (*C*), and direct two-photon absorption (*D*), and also Coulomb explosion (*E*).

Going to higher intensities, Figs. 4(b) and 6(b), the peaks due to dissociation of the vibrational levels $v=2$ and $v=3$, and tentatively also $v=4$ begin to surpass those due to the one-photon absorption. This kind of dissociation is due to three-photon absorption followed by emission of one photon, which in the LIP produces a gap at $v=4$.

(iii) Now we consider the third broad maximum in the velocity region from 8000 to 13 000 m/s. According to the vibrational combs in the speed distributions of Figs. 4 and 6, it is only generated by H and $H+H^+$ fragments, respectively. Looking at Fig. 4, where only neutral H fragments, i.e., dissociation channel (1b) is detected, we clearly identify fragments from $v=10$ and $v=11$ at about 9900 m/s and 10 800 m/s, respectively, in accordance with mainly D fragment signal from these levels in the second broad maximum, see (ii). Also in Fig. 6 where neutrals together with charged

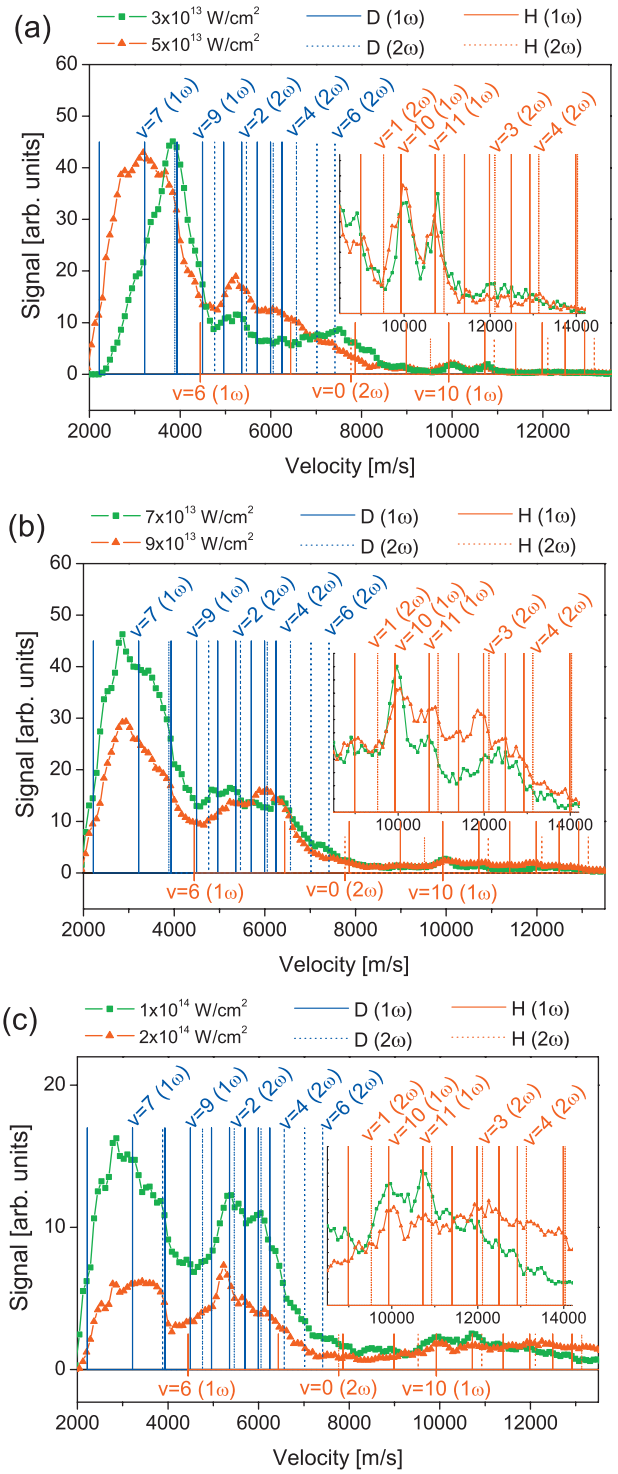

FIG. 6. (Color) Speed distributions of the neutral and charged fragments together for the measurements in Fig. 5. The distributions were obtained by integrating the Abel-inverted velocity distributions over ±4° around the polarization axis at each speed. The vertical lines represent the classically expected velocities for the H and D fragments after one- and net two-photon absorption as calculated from Eq. (4) using field-free energies of vibrational states. The H^+ fragments from the Coulomb explosion channel are around 25 km/s and are not displayed here.

fragments are detected, i.e., both dissociation channels are observed, fragments from these two levels are mainly observed. We also note the broad angular distribution for these fragments, e.g., in Fig. 5, confirming the classical dissociation of these levels.

At higher laser intensities in Fig. 4(b) and Figs. 6(b) and 6(c), the features of $v=3$ and $v=4$ are clearly identified at 12 100 and 13 100 m/s, verifying the three-photon (net two-photon) absorption at high intensities, again in accordance with the D and D^+ fragments' signal in the second maximum. The development of the three-photon (net two-photon) peaks with intensity is best observed in the three-dimensional fragment displays, Figs. 5(a)–5(c).

For the bond softening effect of the levels $v=6-9$, which should also become apparent by the H and H^+ fragments, we must look for the region between 5000 and 8000 m/s. The whole of this region, which mainly displays the classical one- and two-photon dissociation by the D and D^+ fragments as just discussed, is sitting on a broad continuous signal which might be attributed to the bond softening effect as displayed by the H and H^+ fragments. However, it is not possible to ascribe any peaks in this region to this effect.

So far we have detected and discussed the LIP effects such as bond softening as well as classical one- and three-photon (effective two-photon) absorption, all of them leading to dissociation, thereby demonstrating the presence of the gaps at $v=10$ and $v=4$ vibrational levels as suggested by the LIP curves. So far we have a strong analogy of HD^+ to H_2^+ and D_2^+. Here we point out that for the case of only neutral fragments as shown in Figs. 4(a) and 4(b), the two dissociation channels (1a) and (1b) are to a large degree separated. The D fragments on the left-hand side (low velocities) up to about 7000 m/s come from dissociation channel (1a) while the H fragments on the right-hand side (high velocities) all come from channel (1b). There might be an overlap of the two neutral fragments between 7000 and 8500 m/s, see the discussion under (iv).

(iv) The remaining and most interesting question now is the following: Do we see an effect of the direct two-photon absorption in the dissociation being a characteristic of the asymmetric HD^+ molecule? This effect should become apparent due to the induced gap at $v=6$ considering the LIP potential curve system, and consequently by the dissociation of the vibrational levels $v=5-6$ after absorption of two photons, sometimes called "two-photon bond softening." This means that this effect could be detectable corresponding to the D (D^+) vibrational comb for two-photon absorption at the velocities between 7000 and 8000 m/s. Indeed there is a large broad maximum with a double peak structure in the midst at the lowest laser intensities of 3×10^{13} W/cm^2 in Figs. 4(a) and 6(a), and in particular see the three-dimensional display in Figs. 5(a)–5(c), respectively. Unfortunately, also the one-photon bond softening effect due to the one-photon crossing at $v=10$ displayed by the H (H^+) fragments can contribute in the velocity range just mentioned.

This large maximum almost disappears or flattens when going to the next higher intensities in Figs. 4(a) and 6(a). Considering its interpretation by two-photon absorption, this maximum is expected to grow with laser intensity. Its decreasing can be explained by the opening of the one-photon

bond softening channel for the $v=6$ level at these laser intensities which now dominantly depopulates this vibrational level as seen in Figs. 4(a) and 6(a) (red curves). However, also the maximum due to the one-photon bond softening effect displayed by H (H^+) with higher laser intensities would move away from this velocity range to lower velocities which could have a similar consequence. Therefore, we cannot uniquely decide to which degree this broad maximum around 7800 m/s is due to direct two-photon absorption.

However, the small structure around about 7800 m/s coincides exactly with $v=6$ of the two-photon comb and persists for all laser intensities at about the same D (D^+) fragment velocity, perhaps except for the greatest ones used in Fig. 6(b). Since there is also almost no disturbance by other levels, we take this structure as evidence of the two-photon absorption. The weakness of the two-photon absorption effect observed in the spectrum at higher intensities must be attributed to the opening of the one-photon bond softening for $v=6$.

This conclusion is additionally hardened by comparison of our fragment spectrum in Fig. 4(a) to the computer simulated one of Kondorskiy and Nakamura [37] as discussed in Sec. IV H, foreseeing fragments due to the bound-bound-free transitions at the corresponding energy. In particular the shape and width of the broad maximum in Fig. 4(a) between 7000 and 8500 m/s resembles the envelope of the bound-bound-free feature in Fig. 10 of Ref. [37] and completely deviates from the acute shape which would be expected corresponding to the D (D^+) fragments peak around 4000 m/s.

The three-dimensional representations of the fragment distributions in Fig. 5 (left-hand side) illustrate best the competing of the peaks due to the main effects discussed above in (i)–(iv) with laser intensity. From the midst of the distribution outward these are as follows: The bond softening (peak *A*), "classical" one-photon (peak *B*), three- (net two-) photon (peak *C*), and direct two-photon absorption (peak *D*), best seen in Figs. 5(a)–5(d). The direct two-photon peak first surpasses the three-photon peak in Figs. 5(a) and 5(b) until it decreases more and more with further rising intensity, what we interpret as due to the growing of the bond softening effect. All the peaks addressed here are mainly formed here by D (D^+) fragments. Also the opening of the Coulomb explosion channel with increasing laser intensity is observed here by the H^+ and D^+ fragments. The widths of the angular distributions of the different peaks addressed also support here our interpretation in (i)–(iv). This is impressively observed in the three-dimensional diagrams in Figs. 5(c)–5(e).

Concluding the discussion of the radial speed distributions, we point out that this vibrational assignment using the classical vibrational combs and the results of the LIP theory, can only be a qualitative, partly quantitative first step of the interpretation. This must be complemented by an *ab initio* simulation of our radial and angular distributions in Figs. 3–6, starting from the Schrödinger equation, as it was already successfully performed for our measurements on H_2^+ and D_2^+ by Serov *et al.* [44,45] and Kondorskiy and Nakamura [37].

F. Angular distribution of the fragments

As already shown before in Sec. IV E, the study of the angular distribution of the fragments of a certain vibrational level can be of great help to find out the mechanism of its fragmentation.

The dissociation of HD^+ for the classical case, i.e., for the resonant vibrational level $v=10$ which in the LIP picture lies in the crossing, the dipole transition probability of HD^+ from the ground state $1s\sigma^2\Sigma$ to the dissociating first excited state $2p\sigma^2\Sigma$, corresponding to Fermi's golden rule, is proportional to the square of the transition matrix element of the operator $\mathbf{D}\cdot\mathbf{E}\cos\theta$ between the two quantum mechanical states just mentioned. Here the transition dipole moment vector **D** between the two states is parallel to the molecular axis of HD^+, **E** the electric field component of the laser field, and θ is the angle between the vectors **D** and **E**. This means that such a transition is proportional to the laser intensity. Since the axes of the HD^+ molecules are isotropically distributed in space, this leads to a $\cos^2$ distribution of the fragments H (H^+) as well as D (D^+). We shall observe this for the resonantly excited level $v=10$ as we shall discuss.

A much narrower angular distribution of the fragments which can be fitted by a $\cos^n$ curve with $n>2$, is found for the vibrational levels dissociating by bond softening, by more-photon absorption and the ionization channel where the dissociation probability is progressively nonlinear in the laser intensity. This can be understood if we remember that, e.g., in the case of bond softening the dissociation barrier is lowest for molecules with axes parallel to the electric field $(\theta=0)$ and the barrier height increases with increasing angles θ. Correspondingly, the dissociation probability decreases more with increasing angle θ, the higher the power of the intensity I is, leading to a more pronounced angular distribution of the fragments along the laser polarization axis than $\cos^2$. This is usually termed as "geometrical" alignment being mainly determined by the orientation of the dissociating molecules' axes. However, an alignment of the molecules can happen before their dissociation as it can also be the consequence of a dynamical process on the parent molecule: Classically, the electric field exerts a torque on a laser induced molecular dipole moment or, in the case of HD^+, additionally on its permanent electric dipole moment, thereby aligning it into the electric field direction. This process called "dynamical" alignment should play a larger role in our case because of the electric dipole moment of HD^+.

The complete distribution shown so far in Figs. 2 and 3 are the originally measured ones, i.e., they are projections of the spherical fragment velocity distributions onto the detector plane. More exact results can be obtained if these data are Abel inverted to the original spheres. Figure 7 shows angular distributions on such spheres from the reconstructed 3D velocity distributions of the fragments for different vibrational levels. In Fig. 7(a) the angular distribution of the fragments of the vibrational level $v=10$ at a laser intensity of 3×10^{13} W/cm^2 is shown. Since this level lies exactly in the one-photon crossing we expect a classic dissociation according to Fermi's golden rule, and indeed we approximately find a $\cos^2$ angular distribution. In contrast to that, the $v=8$ level lies much lower in the potential curve under the one-photon crossing and should be dissociated by tunneling or passing over the barrier. This is supported by the very narrow distribution measured, indicating nonlinearity in intensity [Fig. 7(b)]. The situation is more complicated when fragments of

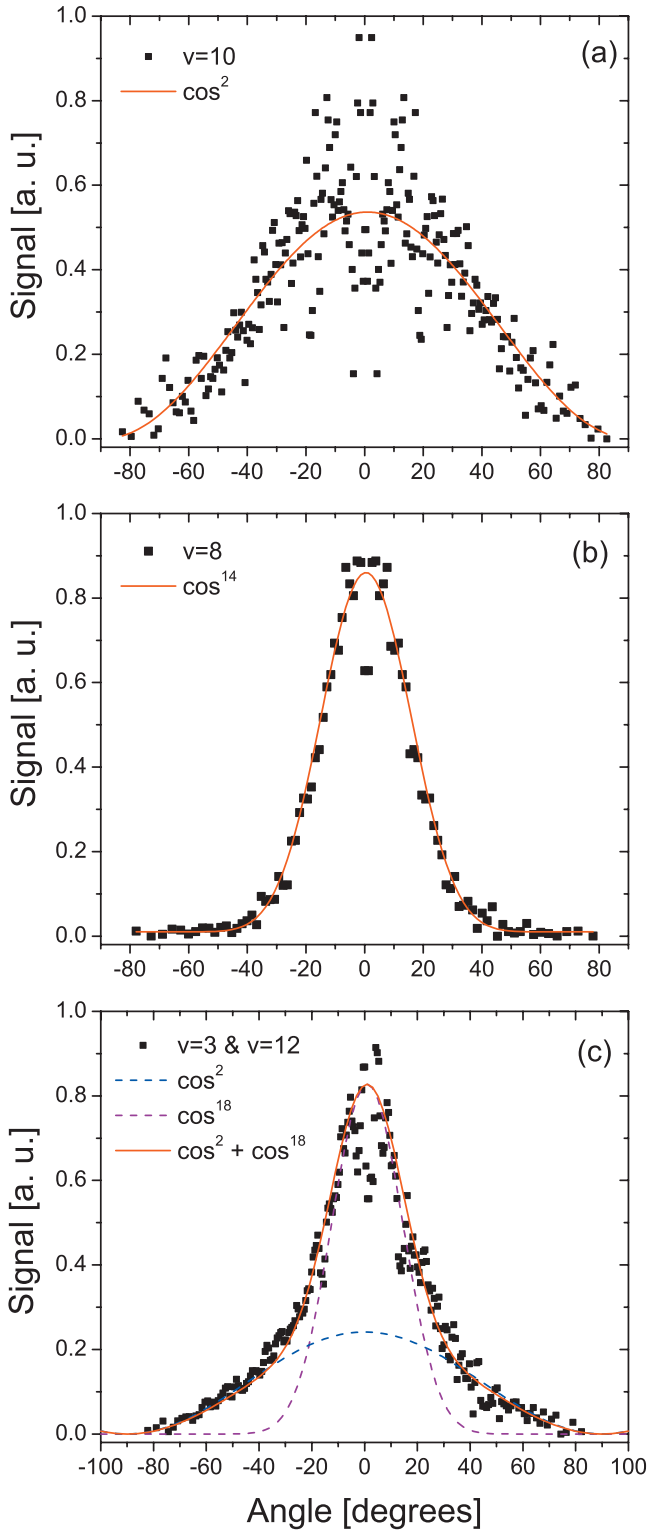

FIG. 7. (Color) Angular distributions of the fragments from different vibrational levels as extracted from the Abel-inverted velocity distributions. The peak laser intensity is 3×10^{13} W/cm^2 in (a) and (b), and 9×10^{13} W/cm^2 in (c). The large scattering of the signal in the midst of the experimental curve is an artifact of the inversion algorithm, resulting from data containing asymmetric contributions.

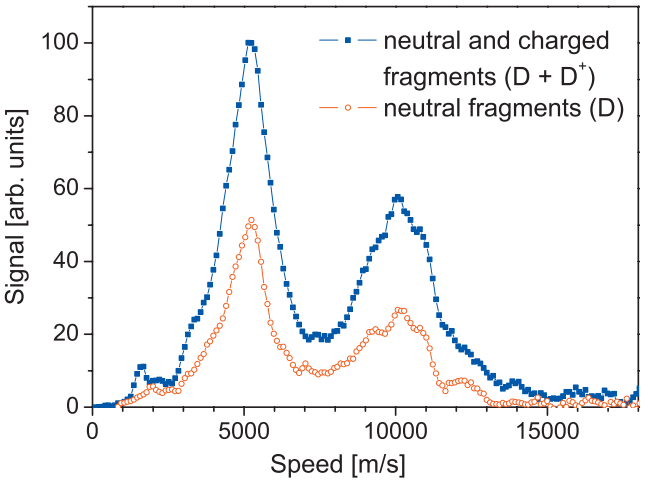

FIG. 8. (Color) Speed distributions for the neutral fragments only and neutral and charged fragments together used for calculation of the branching ratio between the two dissociation channels [Eq. (11)]. The distributions were obtained by integrating the measured velocity distributions over ±45° around the polarization axis and normalizing them by the integrated ion currents (total charges).

vibrational levels dissociated by absorption of one and also more photons energetically coincide, as shown in Fig. 7(c). The narrow upper part and the broad foot of the distribution indicate the contribution of different fragmentation mechanisms. This angular distribution needed a $\cos^2$ and a $\cos^{18}$ curve to be fitted where probably the $\cos^2$ curve fits the $v=12$ part and the $\cos^{18}$ curve the $v=3$ part indicating a classical and a multiphoton mechanism.

G. Asymmetry in the probability of the two dissociation channels

As already discussed, in the case of a breakdown of the Born-Oppenheimer approximation, the two dissociation channels (1a) and (1b) have no longer an equal probability. The first channel mentioned corresponds to a dissociation on the lower $1s\sigma$ potential curve while the second one to a dissociation on the upper $2p\sigma$ curve and they differ in the limit of large R in energy by 3.7 meV [23,26]. This energy difference of the fragments is too small to be resolved by our experimental setup. Therefore a different method was applied to distinguish channels (1a) and (1b): Since the number of D^+ fragments per time interval, $n(D^+)$, represents the probability of the first channel and the number of D fragments per time interval, $n(D)$, that one of the second channel, the fragments were measured switching back and forth between two modi: "Neutrals and charged ones together" and "only the neutrals," in the way it was described before. During the whole measurement the ion current was measured for normalization. In Fig. 8 the plots of the cuts are shown from which the ratio in Eq. (11) was determined. They were obtained by integration over a wide angle of 45 degrees of D and D^+ fragments, respectively, to include as many fragments as possible for the determination of Eq. (11). A velocity range was chosen where almost only D and D^+ were

detected. From the average of all these measurements, the ratio

$$\frac{n(\mathrm{D}+\mathrm{D}^+)}{n(\mathrm{D})} = \frac{n(\mathrm{D})+n(\mathrm{D}^+)}{n(\mathrm{D})} = 1 + \frac{n(\mathrm{D}^+)}{n(\mathrm{D})} \tag{11}$$

was extracted to be 1.06 ± 0.15, which means that the channel $HD^+ \rightarrow H+D^+$ is the preferred one. However, the error of the measurements of about 15% is too large to make a definite decision, though a preference for channel (1b) remains. The main error here was introduced by the measurement of the ion current which had to be performed switching back and forth between the two different Faraday cups. The relative calibration was only possible to 8%. An additional larger error must be attributed to the variation of the laser intensity in the interaction region which could be only partly eliminated. Our result deviates from Ben-Itzhak *et al.* [23] who found the other channel dominant. These two results must not contradict since the two experiments are very different and the overall error in our measurement is too large to conclude something definite. In particular this ratio might depend on the laser intensity. In order to realize the necessary accuracy of less than 1%, appreciable experimental improvements are under way.

H. Comparison to another experiment as well as to a theoretical *ab initio* simulation

To our knowledge there is only one experiment on HD^+ directly comparable to ours, namely the ion beam experiment of Newell *et al.* [46]. Deviating from our experiment, they use a time-of-flight method to measure the kinetic energy and the angular distribution of either the neutral H and D, or the charged fragments H^+ and D^+, without discerning between the two kinds of fragments. They report a $\cos^2$ angular distribution when measuring the two fragments together and integrating over all fragment kinetic energies. They find this is in agreement with their experiments on H_2^+ and D_2^+ and in contrast to neutral H_2 where they find a $\cos^8$ distribution. In our higher resolution measurements, we also find for the neutral D fragments as well as for the H fragments an almost $\cos^2$ distribution for vibrational levels higher than $v=9$, which contribute the greatest part to all fragments. However, for the D fragments from lower vibrational levels, such as $v=6-8$, $\cos^n$ distributions are observed with $n=14$, which was interpreted by the bond softening effect. Also H and D fragments from $v=3$ dissociated by three photons have a narrower angular distribution with $n=18$ [Fig. 7(c)]. As a result, we conclude that the features in the angular distribution characteristic of the intense laser field are only observed if vibrational resolution is reached in the experiment.

Kondorskiy and Nakamura (KN) [37], in their *ab initio* calculation simulated the experimental fragment kinetic energy spectra of H_2^+ reported by Sändig *et al.* [13]. To that aim they solved the Schrödinger equation by a "close coupling method without discretization." The fairly good agreement for the case of H_2^+ with our experiments encouraged these authors to simulate also the fragment kinetic energy spectrum of the mixed isotopomer HD^+ using similar experimental parameters as in the H_2^+ case with the exception of the pulse duration which was chosen to be 65 fs in the case of HD^+. No suitable experimental result was available at that time for comparison.

Comparing the dissociation spectrum of HD^+ calculated by KN to ours, one must respect that on the abscissa the total energy E_{tot} of the dissociating particles is given, unlike our experiment where the fragments' speed w is used.

For the comparison we use

$$E_{\mathrm{tot}} = E_{\mathrm{D}} + E_{\mathrm{H}} = 3E_{\mathrm{D}} = 3/2E_{\mathrm{H}}, \tag{12}$$

$$E_{\mathrm{tot}} = \frac{3}{4} m_{\mathrm{H}} w_{\mathrm{H}}^2, \tag{13}$$

$$E_{\mathrm{tot}} = \frac{3}{2} m_{\mathrm{D}} w_{\mathrm{D}}^2. \tag{14}$$

Here m_{H} and m_{D} are the masses, and w_{H} and w_{D} the velocities in the center-of-mass frame of H (H^+) and D (D^+), respectively.

In our fragments velocity spectrum taken at 3×10^{13} W/cm^2 in Fig. 4(a) (only neutral fragments) and Fig. 6(a) (charged and neutral fragments), the part extending to about 8000 m/s is dominated by deuteron fragments. Therefore, we compare our experimental spectrum to the simulated one of KN, to their Figs. 10 and 11, using Eq. (14) for the transformation of the abscissa. In particular we use for that aim

$$w_{\mathrm{D}} = E_{\mathrm{tot}}^{1/2} \times 0.56 \times 10^4 \ \mathrm{m/s}, \tag{15}$$

which follows from Eq. (14), up to 2.1 eV in their spectrum. Almost all of the peaks in our experimental spectrum find analogs in the simulation of KN with no larger shift on the x axis than a few percent.

Corresponding to KN the peaks up to 1.4 eV in their spectrum are due to one-photon dissociation of the states $v=7-9$. We interpret the range up to 1.5 eV, corresponding to 7100 m/s in our spectrum, being mainly the one-photon fragments from $v=7-12$. We agree with KN that our main peaks at low velocities (energies) are due to bond softening of $v=7-9$.

KN explicitly attribute their spectrum between 1.5 and 2.15 eV to a two-step transition from a deeper band, the first step being a nuclear dipole bound-bound transition characteristic of HD^+, the second dipole transition leading to dissociation. There is a main peak in this part of their simulated spectrum at 1.85 eV with two neighboring ones at 1.74 and 2.1 eV.

The range just mentioned in our experimental spectrum corresponds to a deuteron fragment velocity region from 6900 to 8300 m/s where we see a striking broad bump with a peak at about 7785 m/s which we identify according to Ref. [21] to be the simulated peak at 1.85 eV. Consistently with all that, this peak coincides with $v=6$ and the shoulder there with $v=7$ in our spectrum, both direct two-photon transitions according to our energy comb. They are situated in the avoided crossing of the fictive LIP potential curves sys-

tem, Fig. 1, belonging there to direct two-photon absorption. Furthermore, this region is very little disturbed by other lines.

The small but characteristic peak at 7785 m/s is observed in our different spectra taken at almost all laser intensities. Also the neighboring peaks at 2.0 and 1.75 eV find their analog in some experimental spectra.

Concluding, we are sure to have observed the D (D^+) fragments following the direct two-photon absorption in HD^+ in intense laser fields. As discussed in Sec. IV E, we attribute the relatively weak experimental feature of it which also decreases with increasing laser intensity, to the opening of the one-photon bond softening channel. This begins to deplete the level $v=6$ at an intensity of about 4×10^{13} W/cm^2 and with further growing laser intensity dominates over the direct two-photon absorption. Finally, here we have the interesting observation of two competing intense field effects depleting the same vibrational level, namely $v=6$, which the one-photon (bond softening) effect wins by far against the direct two-photon effect.

In addition we can compare here two two-photon effects where the net two-photon effect being in its first step a three-photon absorption, is more effective here. To be more general, we conclude that the simulation of KN reproduces our spectra quite well and to about a similar degree as our H_2^+ spectra. We must be conscious that for the comparison we attributed the experimental spectrum to D and D^+ fragments, but also contributions of H and H^+ fragments with E_{tot} in the same range are underlying.

Only recently Roudnev and Esry performed *ab initio* calculations on HD^+ [28] as mentioned in the Introduction, thereby also deducing the velocity distribution of the fragments H (H^+) and D (D^+), their Fig. 9. Since they apply a laser pulse shorter by a factor of 10 than used in our experiments, only a qualitative comparison is possible. So, e.g., they find the clear separation of the H (H^+) and D (D^+) fragments. However, the fragment spectra of the two dissociation channels seem to differ much more than in our experiment.

V. CONCLUSION

The isotopically mixed hydrogen molecular ion HD^+ was investigated in intense pulsed laser fields of intensities up to 1×10^{15} W/cm^2 with vibrational resolution, thereby allowing a test of current theories such as LIP for this molecule. In the dissociation spectrum the hydrogen (H, H^+) and deuterium (D, D^+) fragments can almost completely be distinguished because of their very different velocities. Consequently, most of the D (D^+) are arranged more to the midst and most of the H (H^+) more to the outer part of the 2D detector. Most of the peaks discerned can be attributed to fragments coming from certain vibrational levels or groups of unresolved vibrational levels which overlap by shifting and broadening, as in the case of one-photon bond softening, by comparing their kinetic energies to the energy combs respecting the LIP model and the energy partitioning between the H and D fragments. As in the cases of H_2^+ and D_2^+, the LIP effects such as bond softening and level shifting in strong fields, "classical" dissociation obeying Fermi's golden rule as well as two- and three-photon absorption can be verified. The interpretation of these effects is strongly supported by the angular distributions of the fragments in the different vibrational levels.

The three-photon (net two-photon) absorption is observed in plots at higher intensities as peaks close to the expected positions of $v=2-4$ of the two-photon comb by the D (D^+) as well as by the H (H^+) fragments. As expected, the peaks grow and broaden with laser intensity. The direct two-photon absorption peaks at $v=6$ of the two-photon comb, which are characteristic of the asymmetric HD^+ molecule, are larger than the three-photon peaks at the lowest intensities applied. Surprisingly, they decrease with growing intensity until they finally disappear. We identified one-photon bond softening as the reason for this observation. This competing mechanism becomes active at about the intensity of 4×10^{13} W/cm^2, dissociating molecules in the vibrational level $v=6$.

Also the Coulomb explosion channel is observed by its H^+ and D^+ fragments showing the characteristic narrow angular distribution known from the H_2^+ and D_2^+ case. Furthermore, the two dissociation channels of HD^+ can be discerned when measuring only the neutral fragments: The representative fragments H and D appear with very different velocities. By measuring the spectra with and without the charged fragments, the probability for the two channel can be determined. This allows one, in principle, to test Born-Oppenheimer approximation in HD^+, which has been only insufficiently done to date.

So far we could only provide here an interpretation footing on a vibrational assignment of many of the peaks of the radial and angular fragment velocity distribution starting from the classical vibrational combs and LIP results as the basis. We hope that the theoretically working groups supplement this work by *ab initio* simulations of these velocity spectra and angular distributions as it was already done for our H_2^+ and D_2^+ spectra [37,44,45].

[1] A. D. Bandrauk, *Molecules in Laser Fields* (Marcel Dekker, New York, 1994).
[2] J. H. Posthumus and J. F. McCann, in *Molecules and Clusters in Intense Laser Fields*, edited by J. H. Posthumus (Cambridge University Press, Cambridge, 2001), pp. 27–83.
[3] A. Assion, T. Baumert, U. Weichmann, and G. Gerber, Phys. Rev. Lett. **86**, 5695 (2001).
[4] S. Saha, Indian J. Phys. **48**, 849 (1974).
[5] P. R. Bunker, Chem. Phys. Lett. **27**, 322 (1974).
[6] R. E. Moss, Mol. Phys. **97**, 3 (1999).
[7] Z. Amitay *et al.*, Science **281**, 75 (1998).
[8] Z. Amitay, A. Baer, M. Dahan, J. Levin, Z. Vager, D. Zajfman,

L. Knoll, M. Lange, D. Schwalm, R. Wester, A. Wolf, I. F. Schneider, and A. Suzor-Weiner, Phys. Rev. A **60**, 3769 (1999).
[9] T. D. G. Walsh, F. A. Ilkov, S. L. Chin, F. Châteauneuf, T. T. Nguyen-Dang, S. Chelkowski, A. D. Bandrauk, and O. Atabek, Phys. Rev. A **58**, 3922 (1998).
[10] H. Rottke, C. Trump, and W. Sandner, Laser Phys. **9**, 171174 (1999).
[11] C. Wunderlich, H. Figger, and T. W. Hänsch, Chem. Phys. Lett. **256**, 43 (1996).
[12] C. Wunderlich, H. Figger, and T. W. Hänsch, Phys. Rev. A **62**, 023401 (2000).
[13] K. Sändig, H. Figger, and T. W. Hänsch, Phys. Rev. Lett. **85**, 4876 (2000).
[14] I. D. Williams *et al.*, J. Phys. B **33**, 2743 (2000).
[15] D. Pavičić, T. W. Hänsch, and H. Figger, Phys. Rev. A **72**, 053413 (2005).
[16] I. Ben-Itzhak, P. Q. Wang, J. F. Xia, A. M. Sayler, M. A. Smith, K. D. Carnes, and B. D. Esry, Phys. Rev. Lett. **95**, 073002 (2005).
[17] T. Zuo and A. D. Bandrauk, Phys. Rev. A **52**, R2511 (1995).
[18] D. Pavičić, A. Kiess, T. W. Hänsch, and H. Figger, Eur. Phys. J. D **26**, 39 (2003).
[19] D. Pavičić, A. Kiess, T. W. Hänsch, and H. Figger, Phys. Rev. Lett. **94**, 163002 (2005).
[20] A. Kiess, Ph. D. thesis, Ludwig-Maximilians-Universität München, 2003.
[21] A. Kiess, D. Pavičić, T. W. Hänsch, and H. Figger, Verhandl. DPG **39**, A15.19 (2004).
[22] A. Carrington, I. R. McNab, C. A. Montgomerie-Leach, and R. Kennedy, Mol. Phys. **72**, 735 (1991).
[23] I. Ben-Itzhak, E. Wells, K. D. Carnes, V. Krishnamurthi, O. L. Weaver, and B. D. Esry, Phys. Rev. Lett. **85**, 58 (2000).
[24] E. Wells, B. D. Esry, K. D. Carnes, and I. Ben-Itzhak, Phys. Rev. A **62**, 062707 (2000).
[25] E. Charron, A. Giusti-Suzor, and F. H. Mies, Phys. Rev. Lett. **75**, 2815 (1995).
[26] B. Sheehy, B. Walker, and L. F. DiMauro, Phys. Rev. Lett. **74**, 4799 (1995).
[27] V. Roudnev, B. D. Esry, and I. Ben-Itzhak, Phys. Rev. Lett. **93**, 163601 (2004).
[28] V. Roudnev and B. D. Esry, Phys. Rev. A **71**, 013411 (2005).
[29] H. Abou-Rachid, T. Tung-Nguyen-Dang, and O. Atabek, J. Chem. Phys. **110**, 4737 (1999).
[30] A. Carrington, I. R. McNab, and C. A. Montgomerie, J. Phys. B **22**, 3551 (1989).
[31] L. Wolniewicz and J. D. Poll, Can. J. Phys. **63**, 1201 (1985).
[32] F. von Busch and G. H. Dunn, Phys. Rev. A **5**, 1726 (1972).
[33] M. Tadjeddine and G. Parlant, Mol. Phys. **33**, 1797 (1977).
[34] W. H. Wing, G. A. Ruff, W. E. Lamb, Jr., and J. J. Spezeski, Phys. Rev. Lett. **36**, 1488 (1976).
[35] B. Roth, J. C. J. Koelemeij, H. Daerr, and S. Schiller, Phys. Rev. A **74**, 040501(R) (2006).
[36] A. Datta, S. Saha, and S. S. Bhattacharyya, J. Phys. B **30**, 5737 (1997).
[37] A. Kondorskiy and H. Nakamura, Phys. Rev. A **66**, 053412 (2002).
[38] D. Pavičić, Ph.D. thesis, Ludwig-Maximilians-Universität München, 2004.
[39] D. Pavičić, T. W. Hänsch, and H. Figger (unpublished).
[40] R. Bracewell, *The Fourier Transform and Its Applications*, 3rd ed. (McGraw-Hill, Boston, 2000).
[41] M. J. J. Vrakking, Rev. Sci. Instrum. **72**, 4084 (2001).
[42] Information provided by the manufacturer of the MCP detector, Proxitronic GmbH, Bensheim, Germany.
[43] A. Staudte *et al.*, Phys. Rev. Lett. **98**, 073003 (2007).
[44] V. N. Serov, A. Keller, O. Atabek, and N. Billy, Phys. Rev. A **68**, 053401 (2003).
[45] V. Serov, A. Keller, O. Atabek, H. Figger, and D. Pavičić, Phys. Rev. A **72**, 033413 (2005).
[46] W. R. Newell, I. D. Williams, and W. A. Bryan, Eur. Phys. J. D **26**, 99 (2003).